

# Late Cretaceous exhumation of the metamorphic Gleinalm dome, Eastern Alps: kinematics, cooling history and sedimentary response in a sinistral wrench corridor

Franz Neubauer<sup>a</sup>, R. David Dallmeyer<sup>b</sup>, Istvan Dunkl<sup>a</sup>, Dieter Schirnik<sup>a</sup>

<sup>a</sup> *Institute of Geology and Paleontology, Paris-Lodron-University of Salzburg, Hellbrunnerstr. 34, A-5020 Salzburg, Austria*

<sup>b</sup> *Department of Geology, University of Georgia, Athens, GA 30-602, USA*

<sup>c</sup> *Laboratory of Geochemical Research, Hungarian Academy of Sciences, Budaörsi ut 45, H-1112 Budapest, Hungary*

<sup>d</sup> *Institute of Geology and Paleontology, Karl-Franzens-University, Heinrichstr. 26, A-8010 Graz, Austria*

Received 23 May 1993; revised version accepted 10 January 1994

---

## Abstract

The metamorphic Gleinalm dome, Eastern Alps, was uplifted and exhumed within a releasing structure in a sinistral wrench corridor during the Late Cretaceous. The dome is confined by a system of ductile shear zones including low-angle normal faults and steep sinistral tear faults which define a large releasing structure with the metamorphic dome in its center. The fabrics developed within all ductile shear zones record processes which were operating during decreasing temperatures from initial epidote-amphibolite/upper greenschist facies conditions (with crystal plastic fabrics in quartz) to temperatures below ca. 300°C (with predominantly cataclastic fabrics). A cooling path based on <sup>40</sup>Ar/<sup>39</sup>Ar amphibole (95.4 ± 1.2 Ma) and muscovite ages (87.6 ± 0.6; 84.3 ± 0.7 Ma) together with sphene, zircon and apatite fission track data indicate cooling through ca. 500°C at ca. 94 Ma to below ca. 250–200°C at 65 Ma. Subsidence of the adjacent Late Cretaceous Kainach Gosau basin occurred synchronously with cooling and uplift of the Gleinalm dome. Internal depositional patterns record rapid subsidence at the time of cooling with internal synsedimentary block rotation above an intra-crustal ductile normal fault. The sinistral wrench corridor of the Eastern Alps developed by sinistral displacement of the Austroalpine units against a relatively stable Europe during the Late Cretaceous.

---

## 1. Introduction

Several mechanisms have been proposed to contribute to late- to post-orogenic exhumation of crust thickened during collision of continental plates (England and Molnar, 1990). These include: (1) surface erosion (e.g., England and Thompson, 1984); (2) gravitational collapse of overthickened crust (Platt, 1986, 1992; Dewey, 1988); and (3) uplift of upper plate rocks by

underplating (e.g., England and Thompson, 1984; Hsü, 1991). Structural associations have been described which relate rock uplift within metamorphic domes with subsidence of adjacent detachment-related basins (e.g., Coney, 1980; Seguret et al., 1989; Ratschbacher et al., 1989; Echter and Malavieille, 1990; Cassard et al., 1993; Malavieille, 1993). In this paper structural, geochronological and sedimentological data are presented which help to constrain Late Cretaceous rock uplift,

exhumation, and cooling of metamorphic crust exposed within the Gleinalm dome (Figs. 1, 2), and synchronous subsidence within an adjacent, detachment-related Late Cretaceous basin of the Eastern Alps in an overall contractional setting. These results provide insight into the role of wrench translation in tectonic unloading and thinning of overthickened thrust wedges.

## 2. General geological frame

The Austroalpine nappe complex exposed in the central Eastern Alps is mainly composed of imbricated basement thrust units (Fig. 2). Traced tectonostratigraphically downward these include (Tollmann, 1987): (1) Upper Austroalpine units with largely Paleozoic basement and Permian and Mesozoic cover sequences (the latter exposed mainly in the Northern Calcareous Alps; Fig. 2); (2) the Middle Austroalpine units with a Variscan polymetamorphic basement complex (“Altkristallin”), and Permian/Mesozoic cover rocks along northern margins; and (3) Lower Austroalpine units composed of basement and cover sequences forming two major nappes (Grobgneiss and Wechsel nappes).

Internal imbrication of the major Austroalpine units is recorded by Permian and Mesozoic cover

sequences which are structurally interleaved between basement rocks along the northern margins of individual thrust sheets (Fig. 2). Thrusting of Upper Austroalpine over Middle Austroalpine units occurred during the Early and Middle Cretaceous (Ratschbacher, 1986; Krohe, 1987; Frank, 1987; Neubauer et al., 1987; Fritz, 1988; Ratschbacher et al., 1989; Ratschbacher and Neubauer, 1989).

The rocks of the Gleinalm dome are structurally overlain by the Koriden gneiss complex (Fig. 2), another basement unit, which includes Cretaceous eclogites (Thöni and Jagoutz, 1991).

The Gleinalm dome is part of the Muriden complex, a lower basement unit within the Middle Austroalpine units. Rocks of the Gleinalm dome record Alpine upper greenschist facies metamorphic conditions along northern margins. An Alpine lower amphibolite facies metamorphism affected central and southern portions within the Gleinalm dome (Frank, 1987; Neubauer, 1988). Mineral ages previously reported for the Gleinalm dome include (Frank et al., 1976, 1983): Rb–Sr muscovite  $118 \pm 5$  to  $82 \pm 2$  Ma; Rb–Sr biotite  $96 \pm 4$  to  $74 \pm 1$  Ma; K–Ar muscovite  $93 \pm 4$  to  $81 \pm 3$ ; K–Ar biotite  $94 \pm 5$  to  $85 \pm 4$  Ma.

In contrast, Alpine metamorphic conditions within Upper Austroalpine units did not exceed

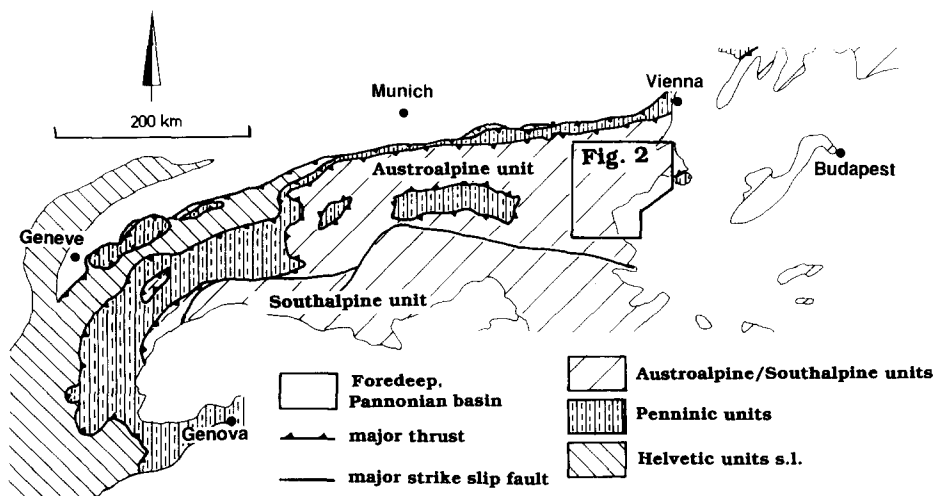


Fig. 1. General tectonic setting of the Alps. The location of the Austroalpine nappe complex is indicated.

middle greenschist facies conditions (e.g., Hasenhüttl and Russegger, 1992). The age of thrusting within the Graz nappe complex (part of the Upper Austroalpine unit) must have predated the late Santonian/early Campanian because of overstepping of internally imbricated units by rocks in the Late Cretaceous Kainach basin (Fig. 2). Furthermore, Rb–Sr and K–Ar ages of minerals, which grew during ductile deformation, indicate Early Cretaceous thrusting within Upper Austroalpine units (Fritz, 1988). An Early Cretaceous age of metamorphism within Upper Austroalpine units is also recorded by a  $139 \pm 6$  Ma lower intercept U–Pb zircon age which has been interpreted to record peak metamorphic greenschist facies conditions (Neubauer et al., 1987).

### 3. Structure of the Gleinalm dome

Middle Austroalpine units are exposed within the Gleinalm dome and its northeastern extensions in the Troiseck–Floning ridge (Fig. 2). The Gleinalm dome is composed of three lithotectonic basement complexes (Neubauer, 1988). Traced tectonostratigraphically upward these include: (1) the Gleinalm “Core” complex with mainly gneiss and amphibolite; (2) the Speik complex with amphibolite and serpentinite; and (3) the Micaschist–Marble complex. The latter is structurally overlain by the Koriden gneiss complex. Units within the Gleinalm dome form NE-trending, dissected antiforms. As a result, the “Core” complex is surrounded by the Speik com-

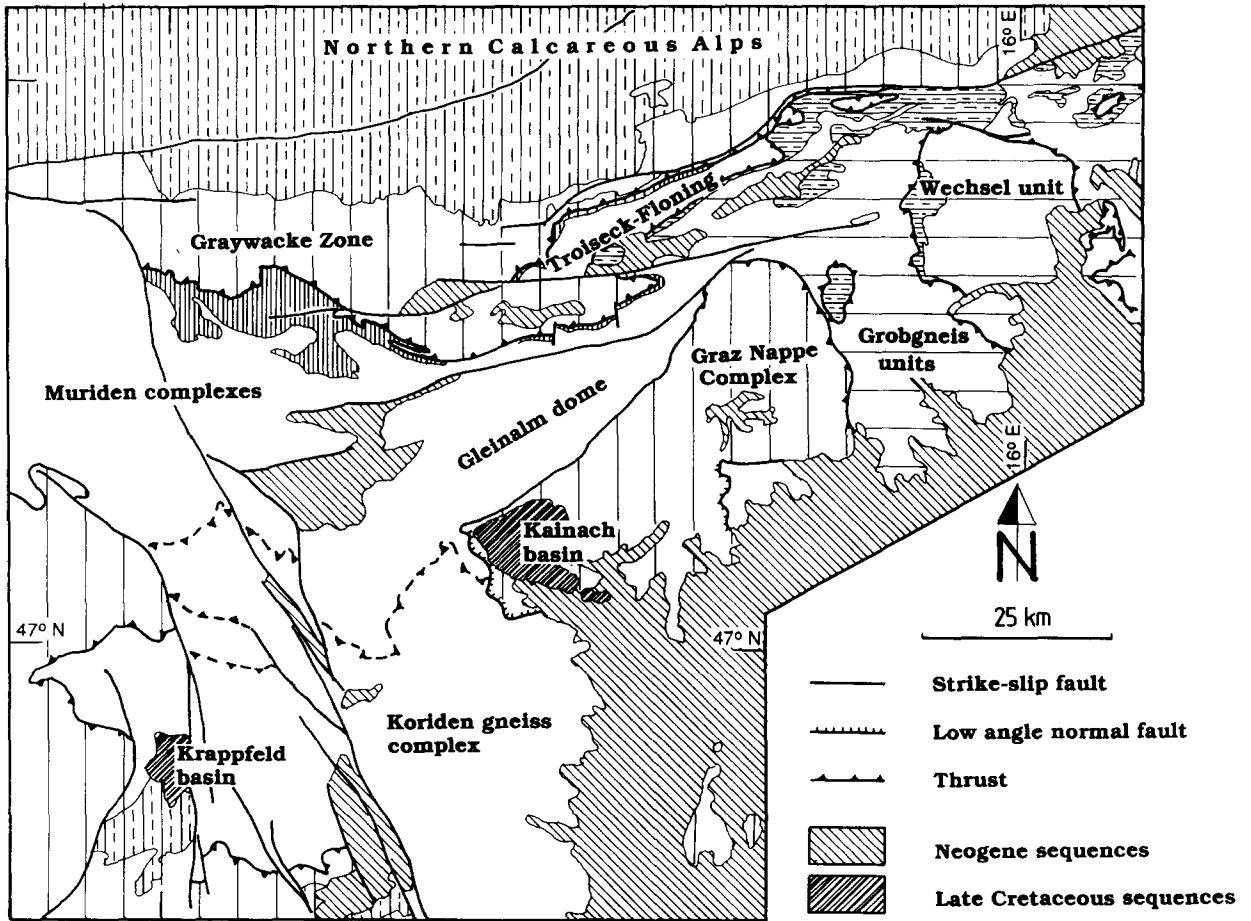


Fig. 2. Simplified tectonic map of the Gleinalm dome and adjacent areas.

plex and the Micaschist–Marble complex (Fig. 3). A broad, W-plunging synform exposes the Speik complex to the north.

The tectonic boundaries of the dome are represented by a system of medium- to high-angle NE-trending ductile shear zones which are partly

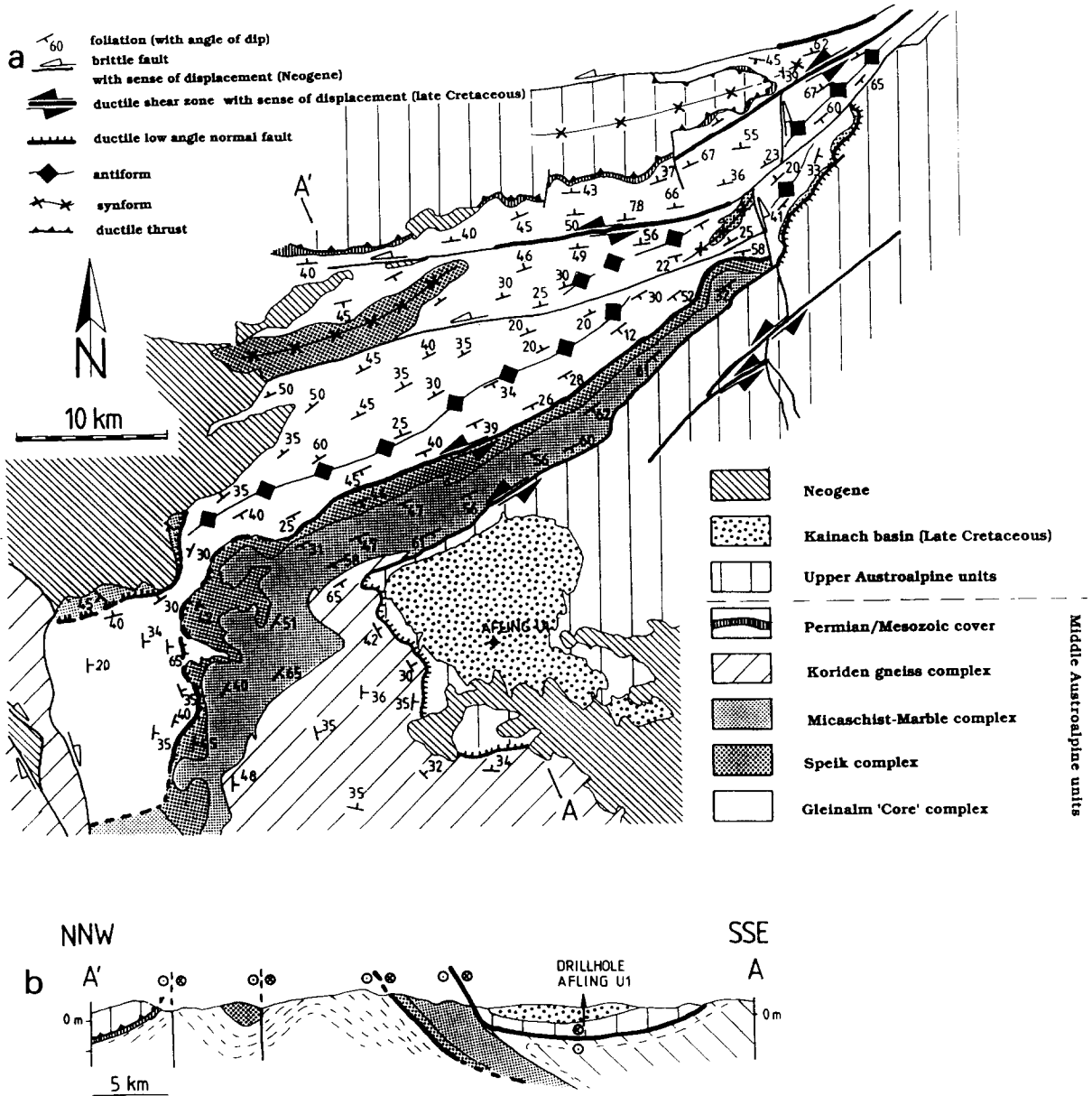


Fig. 3. (a) Tectonic map of the Gleinalm dome displaying an ENE-trending fold structure within the dome, and an interconnected system of steep ductile shear zones and low-angle normal faults along dome margins. The orientation of the composite foliation is shown. For further explanation see text. (b) Generalized cross-section through the Gleinalm dome. For location of the section see (a).

interconnected through a system of low-angle normal faults (Figs. 3a, 4). This system is dissected by ca. E-trending, Neogene strike-slip faults. Several Neogene basins occur along these faults (Nievoll, 1985; Neubauer, 1988; Ratschbacher et al., 1991b). A retrogressive metamorphic overprint was related to confining ductile shear zones along the margins of the dome. The intensity of retrogression increases towards dome margins.

The ductile shear zones have been investigated and re-evaluated using all evidence for sense of displacement (Simpson and Schmid, 1983; Lister and Snoke, 1984; Choukroune et al., 1987; Petit, 1987).

The shear zone on top of the Koriden gneiss complex (Graden normal fault: Fig. 4) is characterized by a gently E-dipping foliation and a flat or NE-plunging stretching lineation. Numerous shear sense indicators (including S–C fabrics, extensional crenulation cleavage, and asymmetric quartz and calcite fabrics) consistently suggest

NE-directed shearing (Krohe, 1987; Fritz et al., 1990; Ratschbacher et al., 1991b). Northeastern extensions of the boundary of the Gleinalm dome into the Graz nappe complex is represented by an about 1.5 to 2.5 km wide medium-angle ductile shear zone (Gleinalm shear zone), which displays an in average 60° SE-dipping foliation and a subhorizontal, in average 10° NE-plunging stretching lineation (Figs. 3a, 4). The sense of shear along this shear zone is always sinistral (Neubauer, 1988). This fault juxtaposes amphibolite facies rocks of the Gleinalm dome against very low- to low-grade units in the Graz nappe complex. The eastern margin of the Gleinalm dome is defined by the ductile Breitenau low-angle normal fault which dips gently to the southeast and displays a northeast-plunging stretching lineation (Figs. 3a, 4). Steeply inclined ductile shear zones were found both along the northern margins and within the Gleinalm dome (Fig. 3a). These shear zones include the Mitterriegler shear zone, and major portions of the Trasattel and

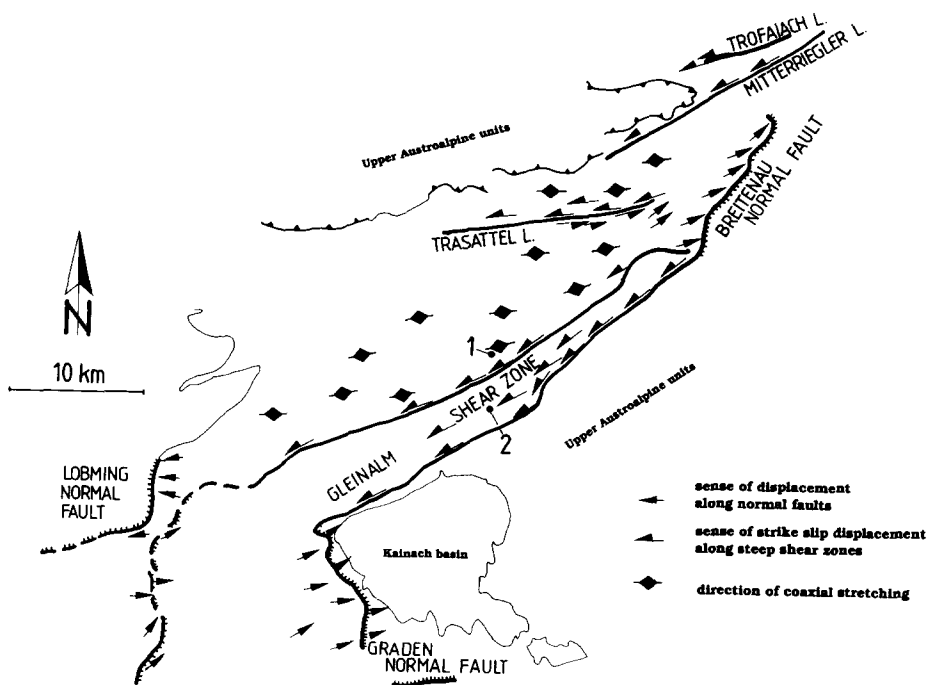


Fig. 4. Indicators for subhorizontal stretching and sense of displacement along late-stage ductile shear zones within the Gleinalm dome. Each datum represents between three and ten observations. Numbers refer to sample localities for <sup>40</sup>Ar/<sup>39</sup>Ar dating.

Trofaiach faults (Fig. 4). The sense of shear is sinistral. These latter two shear zones were reactivated as brittle faults during the Neogene.

The ductile Lobming low-angle normal fault separates imbricated units of the Micaschist–Marble complex from rocks of the Gleinalm



Fig. 5. Representative examples of fabrics characterizing ductile shear zones along upper margins of the Gleinalm dome. (a) Augen gneiss with shear fabrics including recrystallized feldspar grains within feldspar porphyroclast tails formed within upper greenschist to epidote-amphibolite facies conditions along the southeastern margin of the Gleinalm dome (Gleinalm shear zone). (b) Augen gneiss with late-stage cataclastic fabrics in K-feldspar porphyroclasts and plastically deformed quartz ribbon layers from the Mitterriegler line. Scale bar division in both specimen 1 cm.

“Core” complex exposed in the footwall along the northwestern margin of the Gleinalm dome (Figs. 3a, 4). This relationship together with a subhorizontal W-dipping foliation, W-plunging stretching lineation and W-directed sense of shear indicate top-to-the-west transport and a normal fault geometry (Figs. 3a, 4). Deformation was associated with a penetrative retrogression which increases towards the ductile normal fault (Becker and Schumacher, 1973).

Early deformation within all these ductile shear zones was associated with fabrics which include recrystallized potassium feldspar and plagioclase grains (Fig. 5a). This suggests deformational temperatures in excess of ca. 450°C (Tullis and Yund, 1985). Quartz includes dynamically recrystallized grains which display polygonal, equidimensional shapes and later elongated quartz crystals which record little annealing. Final stages of deformation resulted in feldspar cataclasis (Fig. 5b) and sericitization of feldspar.

The interior of the Gleinalm dome displays a set of structures which apparently formed during uplift and cooling. These include discrete, gently E- and W-dipping conjugate shear zones and E- and W-plunging stretching lineations. Mineralized, subvertical tension gashes are common in competent lithologies. The tension gashes generally strike west-northwest suggesting subhorizontal ENE–WSW extension (Fig. 4). Late recumbent folds are locally associated with a weak axial surface foliation. Within central portions of the Hochalpe area to the south of the Trasattel fault, upright, open to tight folds with steep axial surface foliations are widespread. The fold axes trend east and axial surface foliations are subvertical. These relationships suggest that these folds were related to the eastward closure of a large-scale antiform.

#### 4. $^{40}\text{Ar}/^{39}\text{Ar}$ mineral data

$^{40}\text{Ar}/^{39}\text{Ar}$  incremental release age determinations were performed to complement previously published Rb–Sr and K–Ar white mica and biotite ages (Frank et al., 1976, 1983). Samples included: (1) amphibole (sample 1A) and mus-

covite concentrates from the Humpelgraben quarry (sample 1B; for locations see Fig. 4); and (2) a muscovite concentrate (sample 2) from a deformed pegmatite included in the Micaschist–Marble complex near to the southeastern boundary of the complex. Petrographic descriptions of samples are given in Appendix 1. Analytical techniques were similar to those described by Dallmeyer and Gil-Ibarguchi (1990) and Dallmeyer and Takasu (1992). A summary is given in Appendix 2. Analytical results are presented in Table 1 and are portrayed as age spectra in Figs. 6 and 7.

The amphibole concentrate displays a well-defined intermediate- and high-temperature plateau (Fig. 6). These increments display little variation in apparent K/Ca ratios. The argon gas evolved during low temperature increments is highly radiogenic suggesting some extraneous argon present in the amphiboles.  $^{40}\text{Ar}/^{36}\text{Ar}$  vs.  $^{39}\text{Ar}/^{36}\text{Ar}$  correlation of the plateau data is well-defined (MSWD = 1.7). The inverse ordinate intercept is at  $367.5 \pm 45.6$  and suggests little intracrystalline contamination with extraneous argon. Using the inverse abscissa intercept to the age equation yields a plateau isotope correlation age of  $94.1 \pm 1.4$  Ma. This is considered to be geologically significant and is interpreted to date the last cooling through ca.  $500 \pm 25^\circ\text{C}$ , adopting appropriate closure temperatures (e.g., Blanckenburg et al., 1989; Cliff, 1985).

Both muscovite concentrates display similar internally concordant age spectra (Fig. 7). The muscovite concentrate from the Humpelgraben quarry yields a plateau age of  $84.3 \pm 0.7$  Ma, whereas the muscovite concentrate from the second locality (sample 2) records a plateau age of  $87.6 \pm 0.6$  Ma. Also these ages are considered to be geologically significant and are interpreted to date the last cooling through ca.  $375 \pm 25^\circ\text{C}$ .

#### 5. Fission track results

Mineral concentrates of sphene, zircon and apatite for fission track dating (FT) were prepared from the Humpelgraben quarry (location 1

in Fig. 4). The analytical techniques are described in Appendix 3. Results are given in Table 2.

Sphene crystals from the orthogneiss (sample 1C) are tiny, euhedral colorless crystals, whereas those from a paragneiss (sample 1D) are light-yellow to brownish. The number of spontaneous tracks revealed in the colorless samples was significantly higher in the case of the paragneiss.

The orthogneiss sphene did yield an age of  $82.7 \pm 17$ , those of the paragneiss an age of  $69.8 \pm 9.3$  Ma. The zircon concentrate yielded an age of  $61.1 \pm 5.8$  Ma, the apatite  $34.0 \pm 5.6$  Ma.

To get additional information similarly to the TINT and TINCLE procedures widely used for apatite (Lal et al., 1968), 80 track lengths within sphene were determined on the 1D sample. This

Table 1  
 $^{40}\text{Ar}/^{39}\text{Ar}$  analytical data for an incremental heating experiment on a hornblende (sample 1A) and two muscovite (samples 1B, 2) concentrates from the Gleinalm region, Eastern Alps

Release temp. (°C)	$(^{40}\text{Ar}/^{39}\text{Ar})^a$	$(^{36}\text{Ar}/^{39}\text{Ar})^a$	$(^{37}\text{Ar}/^{39}\text{Ar})^b$	$^{39}\text{Ar}$ % of total	$^{40}\text{Ar}$ non-atmos. <sup>c</sup>	$^{36}\text{Ar}_{\text{Ca}}$ %	Apparent age (Ma) <sup>d</sup>
Sample 1A: $J = 0.009925$							
650	27.69	0.04257	2.175	0.99	55.18	1.39	$255.0 \pm 10.6$
750	12.64	0.01766	2.282	1.22	60.13	3.51	$131.4 \pm 12.3$
800	14.76	0.03365	3.836	0.75	34.67	3.10	$89.6 \pm 8.1$
830	10.95	0.02069	4.523	0.66	47.41	5.94	$90.9 \pm 9.2$
855	13.22	0.02205	4.750	0.43	53.55	5.86	$122.8 \pm 14.3$
880	14.66	0.03309	4.237	0.52	35.57	3.48	$91.2 \pm 18.1$
905	15.84	0.03339	4.723	0.65	40.07	3.85	$110.5 \pm 16.2$
930	9.41	0.01044	6.494	2.25	72.70	16.91	$119.0 \pm 8.1$
955	6.42	0.00481	6.754	9.72	86.21	38.16	$96.9 \pm 1.0$
975	5.97	0.00352	7.195	17.96	92.17	55.60	$96.3 \pm 1.0$
990	5.97	0.00331	7.649	18.33	93.79	62.77	$98.0 \pm 1.1$
1000	5.75	0.00341	7.544	8.13	92.90	60.14	$93.6 \pm 1.7$
1010	5.87	0.00508	7.385	4.96	84.45	39.56	$87.0 \pm 1.9$
1070	5.58	0.00296	6.682	16.64	93.83	61.38	$91.7 \pm 1.5$
Fusion	5.84	0.00268	6.557	16.79	95.36	66.52	$97.5 \pm 0.9$
Total	6.52	0.00493	6.870	100.00	89.65	54.00	$98.1 \pm 2.5$
Total without 690–930°C				95.52			$95.4 \pm 1.2$
Sample 1B: $J = 0.009301$							
500	18.07	0.02766	0.035	0.40	54.74	0.03	$158.7 \pm 3.4$
570	8.39	0.00665	0.011	0.46	76.53	0.05	$104.7 \pm 6.2$
620	7.00	0.00366	0.007	0.78	83.63	0.05	$95.6 \pm 11.9$
670	6.03	0.00316	0.003	2.55	84.42	0.02	$83.4 \pm 3.9$
700	5.73	0.00192	0.008	2.92	89.99	0.11	$84.5 \pm 4.9$
730	5.82	0.00205	0.007	3.40	89.49	0.10	$85.4 \pm 2.0$
760	6.32	0.00376	0.004	7.96	82.32	0.03	$85.2 \pm 0.7$
790	5.88	0.00239	0.003	15.51	87.88	0.03	$84.7 \pm 0.6$
820	5.58	0.00147	0.002	19.49	92.12	0.04	$84.2 \pm 0.7$
850	5.83	0.00218	0.004	11.29	88.84	0.05	$84.9 \pm 0.7$
880	5.91	0.00254	0.002	9.18	87.2.0	0.02	$84.5 \pm 1.1$
930	5.73	0.00197	0.002	11.56	89.72	0.03	$84.3 \pm 0.4$
990	5.42	0.00119	0.003	12.87	93.43	0.08	$83.1 \pm 0.6$
Fusion	5.33	0.00010	0.024	1.62	99.39	6.66	$86.8 \pm 4.5$
Total	5.84	0.00220	0.004	100.00	89.23	0.15	$84.9 \pm 1.0$
Total without 500–730°C				87.86			$84.3 \pm 0.7$

Table 1 (continued)

Release temp. (°C)	( <sup>40</sup> Ar/ <sup>39</sup> Ar) <sup>a</sup>	( <sup>36</sup> Ar/ <sup>39</sup> Ar) <sup>a</sup>	( <sup>37</sup> Ar/ <sup>39</sup> Ar) <sup>b</sup>	<sup>39</sup> Ar % of total	<sup>40</sup> Ar non-atmos. <sup>c</sup>	<sup>36</sup> Ar <sub>Ca</sub> %	Apparent age (Ma) <sup>d</sup>
Sample 2: <i>J</i> = 0.008773							
600	12.17	0.01694	0.008	1.85	58.82	0.01	109.8 ± 2.3
670	6.48	0.00275	0.006	4.67	87.38	0.06	87.4 ± 0.8
710	6.13	0.00165	0.007	6.07	91.98	0.12	87.1 ± 0.4
740	6.15	0.00178	0.005	8.40	91.36	0.07	86.7 ± 0.8
770	6.17	0.00181	0.004	10.57	91.23	0.05	86.9 ± 0.3
790	6.13	0.00173	0.002	8.54	91.58	0.03	86.8 ± 0.6
810	6.24	0.00199	0.002	7.21	90.47	0.03	87.2 ± 0.5
830	6.30	0.00206	0.003	6.47	90.25	0.05	87.8 ± 0.5
860	6.32	0.00226	0.001	11.66	89.33	0.01	87.2 ± 0.6
890	6.26	0.00179	0.002	8.95	91.46	0.03	88.4 ± 0.8
930	6.25	0.00156	0.003	9.97	92.54	0.05	89.3 ± 0.4
980	6.21	0.00164	0.003	13.03	92.11	0.05	88.3 ± 0.5
Fusion	6.17	0.00144	0.012	2.61	93.04	0.23	88.5 ± 0.9
Total	6.34	0.00214	0.003	100.00	90.51	0.05	88.1 ± 0.6
Total without 600°C and fusion				95.54			87.6 ± 0.6

<sup>a</sup> Measured.<sup>b</sup> Corrected for post-irradiation decay of <sup>37</sup>Ar (35.1 day 1/2-life).<sup>c</sup> [<sup>40</sup>Ar<sub>tot.</sub> - (<sup>36</sup>Ar<sub>atmos.</sub>) (295.5)]/<sup>40</sup>Ar<sub>tot.</sub><sup>d</sup> Calculated using correction factors of Dalrymple et al. (1981); 2σ intralaboratory errors.

procedure is not routinely used in the case of sphene. A rhyolite sample from the southern Rhodope Massif, Bulgaria, was chosen as a reference material. The track lengths in the 1D sample of the Gleinalm with  $13.1 \pm 0.6 \mu\text{m}$  and of the reference sample with  $13.2 \pm 0.6 \mu\text{m}$  are indistinguishable (Fig. 8). The obtained values perfectly fit with the average length determined by Gleadow and Lovering (1977) in an Australian sphene ( $13.1 \pm 0.6 \mu\text{m}$ ). The Gleinalm sphene track lengths in respect to the rapidly cooled reference sphenes suggest a short period spent within the partial annealing zone. This interval for sphene is approximately between 200 and 300°C. Thus we conclude that the Late Cretaceous cooling was a fast process within this temperature range. This interpretation is supported by a slightly younger zircon age.

The apatite FT age is much younger than all of the other geochronological results. The determined  $34 \pm 6 \text{ Ma}$  is an apparent age. The crystals only contain six confined tracks in horizontal position which ranges between 10.5 and 16  $\mu\text{m}$  and the average of  $13.1 \pm 2 \mu\text{m}$  apparently indi-

cates a significant amount of shortening, revealing later reheating within the partial annealing zone of apatite.

## 6. Metamorphic conditions and cooling path

Peak conditions of Alpine metamorphism within central and southern sectors of the Gleinalm area are, in part, constrained by the presence of kyanite in metapelites. This indicates that peak-temperature conditions and subsequent retrogression occurred within the stability field of kyanite (Fig. 9). Common mineral assemblages of amphibolites include green amphibole, plagioclase, quartz, clinozoisite and sphene with variable contents of chlorite. This assemblage indicates epidote-amphibolite facies conditions. Retrogressive greenschist facies mineral assemblages prevail near the boundaries of the metamorphic dome. They are dominated by pale amphibole/actinolite + epidote + chlorite + biotite within amphibolites. The <sup>40</sup>Ar/<sup>39</sup>Ar amphibole date obtained from the Humpelgraben quarry ( $94.1 \pm 4$

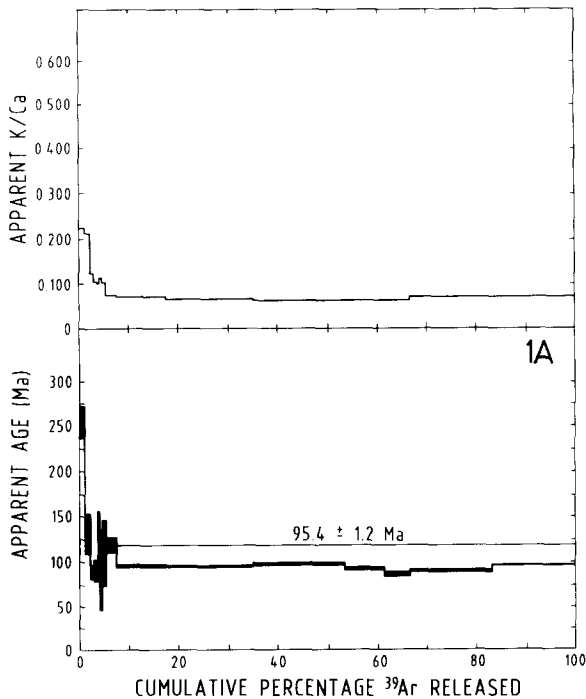


Fig. 6.  $^{40}\text{Ar}/^{39}\text{Ar}$  incremental release spectrum and apparent K/Ca spectrum of an amphibole from the Gleinalm "Core" complex, Humpelgraben quarry. Analytical uncertainties ( $2\sigma$  intralaboratory) are represented by vertical width of scale bars. Experimental temperatures increase from left to right.

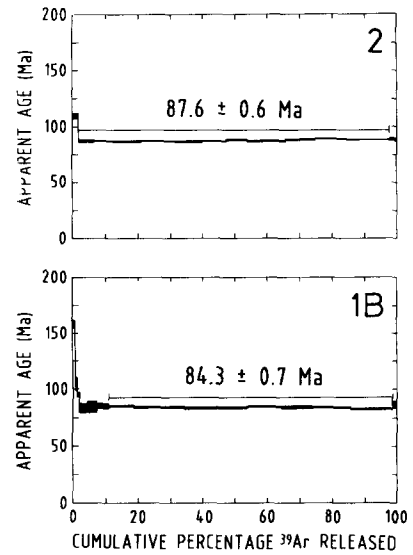


Fig. 7.  $^{40}\text{Ar}/^{39}\text{Ar}$  incremental release spectra of two muscovite concentrates from the southern Gleinalm area. Analytical uncertainties ( $2\sigma$  intralaboratory) are represented by vertical width of scale bars. Experimental temperatures increase from left to right.

Ma) suggests complete Alpine rejuvenation with peak temperatures in excess of ca.  $500^\circ\text{C}$ .

Comparison of the  $^{40}\text{Ar}/^{39}\text{Ar}$  amphibole and

Table 2  
Fission track results from the Gleinalm dome, Humpelgraben quarry

Sample	Number of crystals	$P_s$	$(N_s)$	$P_i$	$(N_i)$	$P$ (%)	$P_d$	$N_d$	Fission track age $\pm 2\sigma$ (Ma)
Sphene:									
1C	7	23.6	(369)	18.2	(280)	1	3.99	(9969)	$82.7 \pm 17$
1D/a	10	58.3	(1457)	85.6	(2140)	< 1	6.35	(11304)	$67.7 \pm 9.5$
1D/b	10	62.4	(1328)	85.6	(1816)	< 1	6.35	(11304)	$72.1 \pm 10$
								1D sphene:	$69.8 \pm 9.3$
Zircon:									
1C	24	137	(3498)	46.1	(1161)	5	1.16	(4346)	$61.1 \pm 5.8$
Apatite:									
1D	50	0.16	(202)	0.74	(891)	81	6.35	(11304)	$34.0 \pm 5.6$

Spontaneous ( $P_s$ ) and induced track densities ( $P_i$ ) of the samples and of the detector ( $P_d$ ) are as measured and are ( $\times 10^5$  tracks/cm $^2$ ). Numbers of tracks counted ( $N_s$ ,  $N_i$ ,  $N_d$ ) are shown in brackets.  $P$  (%): chi-square probability for  $n - 1$  degrees of freedom (where  $n$  = number of crystals). Ages are calculated using the zeta method and standard glass SRM 612. Zeta for apatite  $488 \pm 13$ , for zircon  $370 \pm 11$  and for sphene  $328 \pm 20$  were used

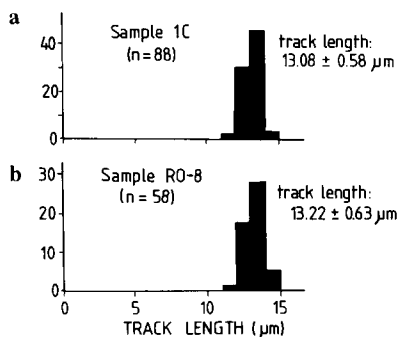


Fig. 8. Lengths of sphene fission tracks of the Gleinalm sample 1D (a) and from a rhyolite from the Rhodope Massif (b), Bulgaria, for reference of a rapidly cooled rock.

muscovite and fission track data with previously published Rb–Sr and K–Ar muscovite and biotite data from the Humpelgraben quarry (Frank et al., 1976, 1983) allows the calibration of the post-metamorphic cooling path for the “Core” complex (Fig. 10). We adopt appropriate closing temperatures for amphibole (ca. 500°C after Harrison, 1981) and the Rb–Sr and K–Ar isotopic systems in muscovite (ca. 375 ± 25°C) and biotite (300°C; e.g., Cliff, 1985; Blanckenburg et al., 1989).

The above presented mineral ages record a cooling from ca. 500°C at ca. 95 Ma to 225°C at ca. 61 Ma, with an average cooling rate of ca. 9°C/Ma.

### 7. Sedimentation history within the Kainach basin

The Late Cretaceous Kainach basin is exposed southeast of the Gleinalm dome. The Kainach basin is separated by several hundred metres thick, slightly metamorphic Upper Austroalpine rocks from the underlying Gleinalm dome (Fig. 3a). The stratigraphic range of the Kainach basin fill is late Santonian to Maastrichtian (van Hinte, 1965; Kollmann, 1965; Pamouktchiev, 1970; Gräf, 1975; Ebner, 1986).

Six major lithofacies units (Fig. 11) have been recognized (Schirnik, 1994). Stratigraphically upwards these include the following:

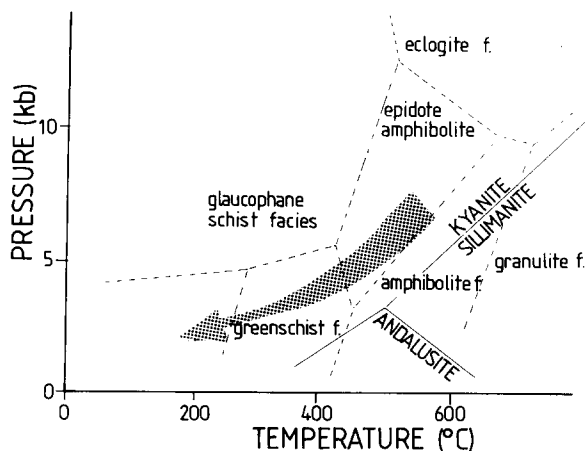


Fig. 9. Suggested Alpine P–T conditions within the Gleinalm dome. Simplified petrogenetic grid of mafic rocks and the stability fields of Al<sub>2</sub>SiO<sub>5</sub> polymorphs (Holdaway, 1971) are shown.

(1) A proximal alluvial facies which is a massive to horizontally stratified, clast-supported reddish pebble to boulder conglomerate.

(2) A distal alluvial facies which mainly contains horizontally and cross-stratified pebble conglomerates/sandstones and red to green siltstones/mudstones in fining-upward channel fills

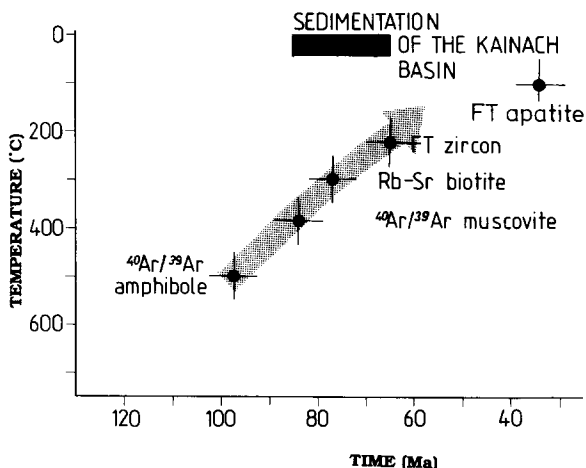


Fig. 10. Cooling path of the Gleinalm “Core” complex within the Gleinalm dome based on relationships in the Humpelgraben quarry. Time interval of sedimentation within the Kainach basin is shown using the time calibrations of Harland et al. (1990).

with incipient soils (calcrete) in flood plane areas. We interpret this lithotype as derived from density-modified grain flows or from longitudinal medial bars.

(3) A lacustrine facies which comprises subaqueous mass flow conglomerates/sandstones and turbiditic sandstones in distal delta parts, prodelta of varved mudstones and marls with abundant sliding and slumping.

(4) A coarse submarine fan-delta facies (according to the model of Nemec and Steel, 1988) which include wave-reworked mouth bar conglomerates (beachface, shoreface) and transgressive lag conglomerates. These conglomerates grade upwards into mass flow boulder conglomerates passing into finer-grained mass flow conglomerates which are interbedded with turbiditic sandstones and parallel-laminated mudstones in both fining upward and coarsening-upward sequences.

(5) Well sorted sandstones of a fine-grained fan-delta facies equal with the former. These sandstones often contain low-angle beach stratification and wave-reworked structures (Clifton, 1969).

(6) A distal submarine fan-delta facies (Hauptbecken Formation: Gräf, 1975) is composed of fine-grained turbiditic sandstones/pebbly conglomerates. This facies turns in the central/northern part from conglomeratic mass flows into fine-grained parallel-laminated mudstones with only minor intercalations of thin-bedded turbiditic sandstones. In the western part, the fine-grained mudstones and intercalated pebbly mudstones/sandstones contain abundant evidence for slumping and sliding.

All the lithofacies data together represent an evolution from a coarse alluvial facies, through a lacustrine shallow-water fan delta to a marine slope-type fan-delta system with interbed basin sedimentation (Wescott and Etheridge, 1980; Etheridge and Wescott, 1984).

Sediment transport directions ranged from northeast to northwest in lower lithofacies units, but were only northeast in the upper part (Fig. 11). The clastic detritus is derived from three sources (Gollner et al., 1987): (1) sedimentary and volcanic rocks which closely resemble sequences of the surrounding Paleozoic of Graz; (2) dominant clasts are Permian–Mesozoic rocks

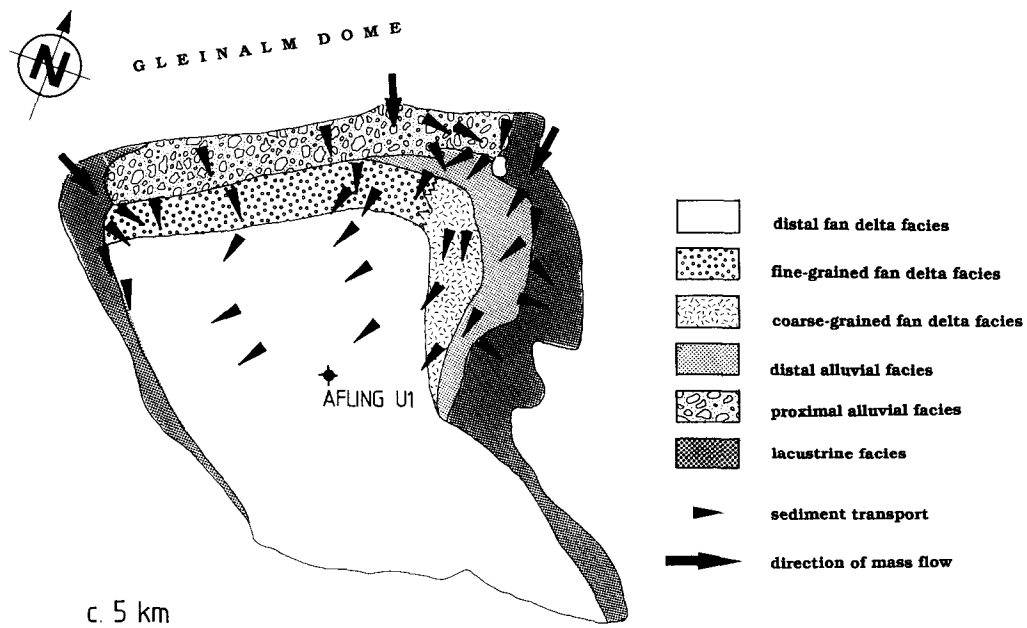


Fig. 11. Distribution of sedimentary lithofacies within the Kainach basin.

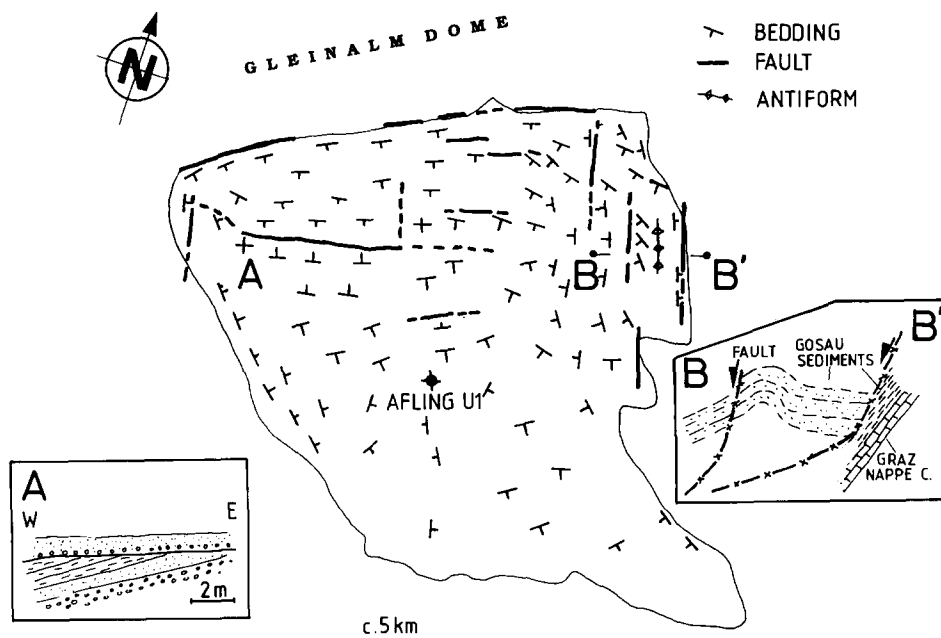


Fig. 12. Schematic structural map of the Kainach basin.

similar to those presently exposed in the Northern Calcareous Alps; (3) Permian–Mesozoic clasts, e.g. Permian fusulinid-bearing limestones, from the Southalpine unit. Metamorphic clasts which could be derived from the surrounding Altkristallin do not occur within the Kainach basin.

The overall structure of the Kainach basin is an asymmetric basin-like structure with a structural thickness, controlled by the well U1 Afling (Kröll and Heller, 1978), of ca. 1,000 m in the central part. Because of a low, limited tilting to the east in the western part, the thickness reaches ca. 1600 m. Tilting of the easternmost third of the basin to the west suggests stratigraphic thickness of ca. 2500 m in the eastern part (Figs. 11, 12).

We interpret the eastern portion of the Kainach basin deposits to represent a prograding/retrograding fan-delta system, and the western portion as a retrograding fan-delta system. The skewed fan body in the eastern part indicates slowed subsidence rates in the eastern part. The

deposition of all described lithofacies types indicates a strongly aggrading system with average sedimentation rates of 20–40 cm/1000 yr.

Westward basin floor tilting is indicated by: (a) unconformities in outcrops (Fig. 12A) as well as in the drill hole Afling U1 (Kröll and Heller, 1978); (b) westward-directed sediment transport directions in the upper parts of sections (Fig. 11); and (c) abundance of slumps in the western sectors of the distal fan-delta facies. Extension is also proved by W-dipping normal faults in eastern portions of the basin (B in Fig. 12).

Major tectonic pulses which are responsible for subsidence occurred during: (a) the late Santonian (start of subsidence); (b) approximately the early Campanian (marine transgression); and (c) the Maastrichtian (angular unconformities within the slope-type fan-delta facies).

Paleomagnetic studies of Gosau sediments showed broadly and unsystematically varying paleopoles of remanent magnetism (Agnoli et al., 1989). Vitrinite reflectance studies suggest post-

depositional thermal conditions of ca. 180°C within basal formations of the Gosau basin (Teichmüller, 1980).

**8. Discussion**

Essentially the Austroalpine crust within the Gleinalm dome records synchronous cooling and uplift of metamorphic crust within the dome with subsidence and sedimentation in the adjacent

Kainach basin. Similar relationships between uplift of metamorphic sequences and subsidence of adjacent basins during late-orogenic, lithospheric extension were observed in several orogens like the Norwegian Caledonides (Seguret et al., 1989; Chauvet and Dallmeyer, 1992), the French Variscides (Echtler and Malavieille, 1990) and during the Neogene in the Alps (Ratschbacher et al., 1989). A major difference exists in the role of strike-slip faults which apparently dominate the structural setting of the Gleinalm dome.

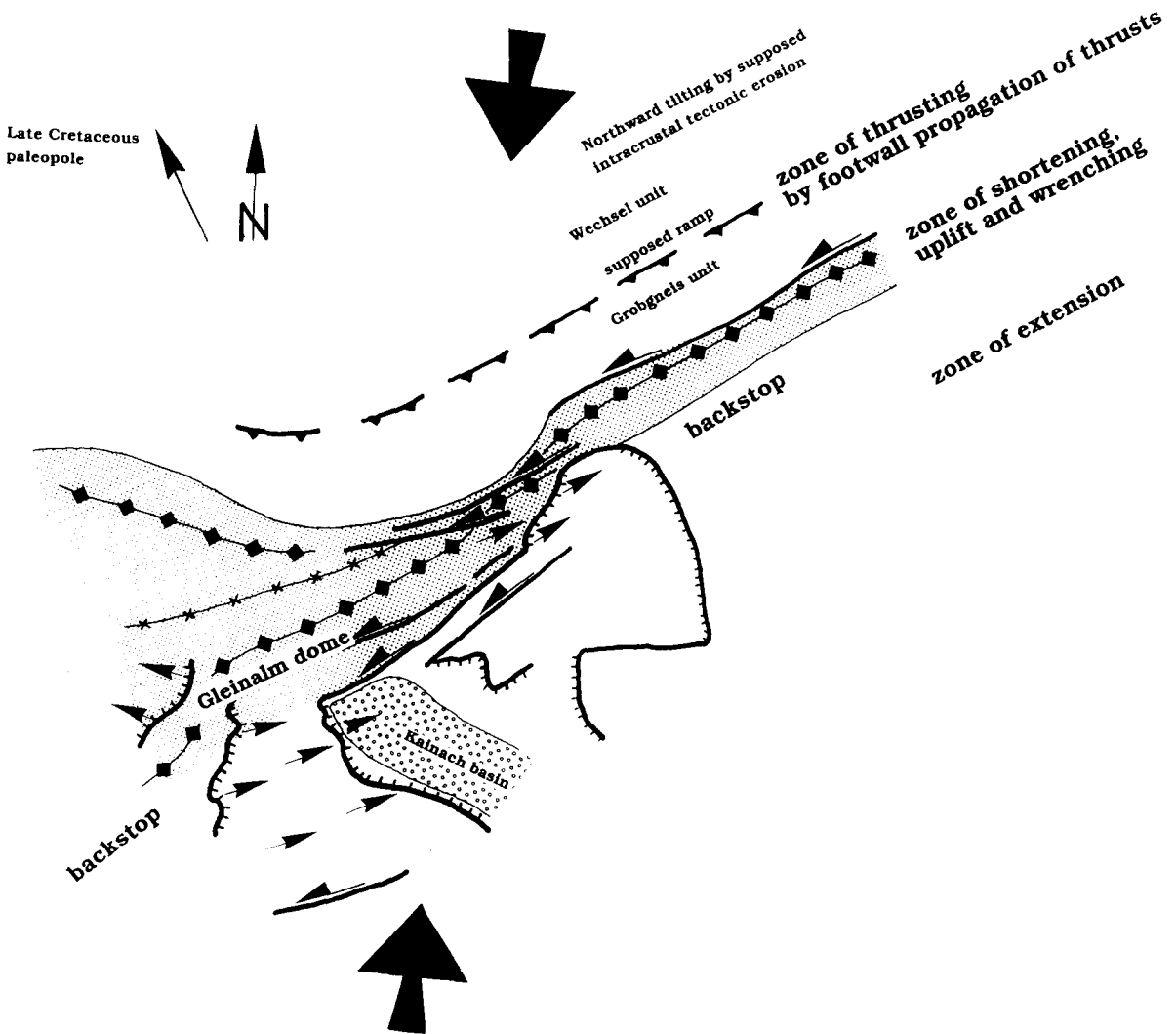


Fig. 13. Kinematic model of the uplift history of the Gleinalm dome. For explanation see text.

Uplift and cooling of the metamorphic Gleinalm dome was accommodated by a system of interconnected strike-slip and low-angle normal faults which were also responsible for subsidence of the Kainach basin within a releasing bend. The W-directed Lobming and the NE-directed Breitenau normal faults which apparently have been operating during the same time interval during cooling suggest WSW–ENE-stretching of the entire Gleinalm dome. Similar extension deduced by fault patterns was reported by Ratschbacher et al. (1991a) within the Kainach basin although these structures postdate basin fill. The subsidence of the Kainach basin was controlled by similar kinematics as expressed in the Graden normal fault and the Gleinalm shear zone. The steep sinistral, NE-trending shear zones suggest subhorizontal contraction in about a north–south direction. The most reliable orientation of contraction within the Gleinalm dome is marked by subvertical mineralized N- to NNW-trending tension gashes which formed during cooling of the dome. Furthermore, subvertical shortening is indicated by recumbent folds which are associated with a flat-lying axial surface foliation. Such folds have been described in a number of extensional settings (e.g., Froitzheim, 1992). Antiformal bending of the dome must have resulted from contraction. This most likely was accommodated by shortening of a rock mass above a shear zone, e.g. a thrust fault, at depth. Thrust faults between Middle and Lower Austroalpine as well as within Lower Austroalpine units could have operated as contractional faults which accommodated contraction of the Gleinalm dome (Fig. 13). Thrust faults responsible for intra-Lower Austroalpine nappe imbrication display N-directed displacement (Reindl, 1989; Neubauer et al., 1992) dated at ca. 80–70 Ma by Rb–Sr and  $^{40}\text{Ar}/^{39}\text{Ar}$  muscovite ages (Frank et al., 1987; Dallmeyer et al., 1992; Mueller et al., 1992). Northward-directed nappe stacking within Lower Austroalpine units was related to formation of basement ramps during which the basement (Grobgnais unit) did override the supracrustal Wechsel unit. Therefore, we conclude that uplift and extension of the Gleinalm dome was related to contemporaneous crustal shortening within lower levels of the oro-

genic wedge, the Lower Austroalpine units (Fig. 13). This process was apparently contemporaneous to northwestward-tilting of the Upper Austroalpine nappe succession within the Northern Calcareous Alps which is supposed to record subcrustal tectonic erosion beneath the nappe stack (Wagreich, 1991, 1995). In a north–south section across the Cretaceous orogenic wedge within the Eastern Alps three zones may be distinguished (Fig. 13): (1) a northern zone of active thrust propagation and thickening of crust and later, southerly prograding subcrustal erosion which we relate to climbing of master thrust faults into Permian/Mesozoic cover sequences; (2) a zone of crustal shortening, uplift and orogen-parallel wrenching-induced extension; and (3) a southern zone with predominant extension and ductile thinning of crust. This zone is apparently separated from the Gleinalm dome by a sort of backstop within the orogenic wedge.

The Kainach basin unconformably overlies Upper Austroalpine units. A ductile low-angle normal fault was located along the hangingwall boundary of the Koriden gneiss complex. This portion of the Koriden gneiss complex grades towards the south into eclogite-bearing rock for which  $P$ – $T$  conditions of ca. 600°C and 14–18 kbar were estimated (Miller, 1990). Sm–Nd mineral ages indicate an Alpine age of eclogite metamorphism (Thöni and Jagoutz, 1992). Krohe (1987), Fritz et al. (1990) and Ratschbacher et al. (1991b) described ductile low-angle normal faults which were responsible for the formation of the Kainach Gosau basin. Clast compositions within the Kainach basin indicate erosion of a Permo–Mesozoic cover sequence and, likely later, erosion of very low-grade metamorphic basement. Observed directions of sediment transport suggest the erosion of a ridge located immediately north of the present basin. Occurrences of Southalpine clasts suggest linkages with drainage systems of Southalpine units.

The evolution of the Kainach basin appears to have occurred in three stages (after models of Reading, 1982, 1986): (1) subsidence by low-angle normal faulting; (2) filling of the basin during synsedimentary subsidence indicated by an apparent rollover structure; and (3) basin inversion

and uplift by subsequent compression during continuing strike-slip motion during which basal portions of Gosau sediments were displaced along the Gleinalm shear zone.

Subsidence history and lithofacies distribution argue for a marked tectonic subsidence during early stages of basin history. The main subsidence occurred during the late Santonian to early Campanian and was associated with a marked change from alluvial and lacustrine sedimentation to fan-delta deposits. Maastrichtian sequences may record the basin fill after tectonic subsidence.

Similar structural relationships between an uplifted metamorphic dome and adjacent sedimentary basins developed in late stages of orogenic evolution have been described in a number of orogens. These include: the Basin and Range Province of western North America (Coney, 1980), the Norwegian Caledonides (e.g., Seguret et al., 1989; Chauvet and Dalmeyer, 1992), and the Montagne Noire in France (Echtler and Malavieille, 1990; Cassard et al., 1993). In all these examples wrenching apparently connects uplift of metamorphic domes with subsidence of adjacent basins.

Of major interest is the evidence for sinistral wrenching in the Eastern Alps during the Late Cretaceous. Such wrenching fits well into a number of independent evidences which come from the opening history of the Atlantic Ocean. All authors agree that the time between ca. 140 and 80 Ma is a time with a large contraction between Africa and stable Eurasia combined with a sinistral component of offset (Le Pichon et al., 1988; Dewey et al., 1989). The sinistral displacement is interpreted to be related to the opening of the North Atlantic Ocean during which an eastward shift of Iberia along the North Pyrenean fault resulted in some sinistral displacement in the Alps. This wrench component may have resulted in the formation of steep ductile shear zones along the margins of the Gleinalm dome.

## 9. Conclusions

Cooling and uplift of the Gleinalm dome was obviously related to contraction along deep-seated

thrusts. Oblique contraction resulted in partitioning of deformation into thrusting at deep crustal levels, and wrenching and normal faulting perpendicular to shortening direction at mid-crustal levels. Uplift of metamorphic domes is accomplished by steps along the wrench system. Complementarily, the subsidence of the adjacent basin is the result of a releasing structure. The structural association argues for a geometrical control of the extensional structures during oblique shortening rather than by gravitational collapse.

## Acknowledgements

The model is based on many fruitful discussions with Wolfgang Frisch, Harry Fritz, Hans Genser and Lothar Ratschbacher. We gratefully appreciate careful reviews by Lothar Ratschbacher and Stefan Schmid. Grass helped with support during irradiation of fission track samples. We acknowledge support by a grant of the Austrian Research Foundation (P7405, 8652) to F.N., by a grant (EAR-9316042) from the Tectonics Program of the U.S. National Science Foundation to R.D.D., and by the Hungarian National Research Found (OTKA 232/1991–1994) to I.D.

## Appendix 1

*Sample 1A:* abandoned Humpelgraben quarry. Fine-grained foliated amphibolite with strong mineral lineation formed by amphiboles. Amphiboles are green and do not display optically detectable internal zoning. The matrix is composed of fine-grained aggregates of plagioclase, and subordinate quartz, garnet, sphene, clinozoisite, biotite and opaque minerals. Garnet forms relics which are surrounded by mostly plagioclase, biotite, quartz, and little bluish-green amphibole.

*Sample 1B:* abandoned Humpelgraben quarry. Medium-grained Humpelgraben granite gneiss. The well-foliated rock consists of plagioclase, K-feldspar with myrmekitic patches along margins, quartz, muscovite, biotite, garnet, and zircon and apatite as accessories. The foliation is formed by mica flakes, and elongated quartz grains which include subgrains along margins.

*Sample 2:* road exposure ca. 2 km west of the mouth of the Kleintal stream into the Neuhof valley. The mylonitic peg-

matite contains cm-sized books of muscovite of magmatic origin and mm-sized recrystallized metamorphic muscovite, the later forming an anastomosing foliation. The mm-sized muscovite was concentrated for  $^{40}\text{Ar}/^{39}\text{Ar}$  analysis. Further major rock constituents are alkali feldspar, plagioclase and quartz. All of them occur in two generations, namely in porphyroclasts of originally magmatic origin and recrystallized grains of metamorphic origin.

## Appendix 2

Mineral concentrates for  $^{40}\text{Ar}/^{39}\text{Ar}$  analysis were wrapped in aluminium-foil packets, encapsulated in sealed quartz vials, and irradiated for 40 h in the central thimble position of the TRIGA Reactor at the U.S. Geological Survey, Denver. Variations in the flux of neutrons along the length of the irradiation assembly were monitored with several mineral standards, including hornblende MMhb-1 (Samson and Alexander, 1987). The samples were incrementally heated until fusion in a double-vacuum, resistance-heated furnace. Temperatures were monitored with a direct-contact thermocouple and are controlled to  $\pm 1^\circ\text{C}$  between increments and are accurate to  $\pm 5^\circ\text{C}$ . Measured isotopic ratios were corrected for total systems blanks and the effects of mass discrimination. Interfering isotopes produced during irradiation were corrected using the factors reported by Dalrymple (1981) for the TRIGA Reactor. Apparent  $^{40}\text{Ar}/^{39}\text{Ar}$  ages were calculated from corrected isotopic ratios using the decay constants and isotopic abundance ratios listed by Steiger and Jäger (1977) following the methods described in Dallmeyer and Keppie (1987).

Intralaboratory uncertainties are reported and have been calculated by statistical propagation of uncertainties associated with measurement of each isotopic ratio (at two standard deviations of the mean) through the age equation. Interlaboratory uncertainties are ca.  $\pm 1.25$ – $1.5\%$  of the quoted age. Total-gas ages have been computed for each sample by appropriate weighting of the age and percent  $^{39}\text{Ar}$  released within each temperature increment. A “plateau” is considered to be defined if the ages recorded by two or more contiguous gas fractions each representing  $> 4\%$  of the total  $^{39}\text{Ar}$  evolved (and together constituting  $> 50\%$  of the total quantity of  $^{39}\text{Ar}$  evolved) are mutually similar within a  $\pm 1\%$  intralaboratory uncertainty. Analysis of the MMhb-1 amphibole monitor indicates that apparent K/Ca ratios may be calculated through the relationship  $0.518 (\pm 0.005) \times (^{40}\text{Ar}/^{39}\text{Ar})(^{39}\text{Ar}/^{37}\text{Ar})_{\text{corrected}}$ .

Plateau portions of the analyses have been plotted on  $^{36}\text{Ar}/^{40}\text{Ar}$  vs.  $^{39}\text{Ar}/^{40}\text{Ar}$  isotope correlation diagrams (Roddick et al., 1980; Radicati di Brozolo et al., 1981). Regression techniques followed the methods of York (1969). A mean square of the weighted deviates (MSWD) is the statistical parameter which has been used to evaluate isotopic correlations. Roddick (1978) suggests that an MSWD greater than ca. 2.5 indicates scatter about a correlation line greater than that which can be explained only by experimental errors.

## Appendix 3

Sphene, zircon and apatite crystals were concentrated from the 70–180  $\mu\text{m}$  sieve fraction by heavy liquid and magnetic separation. Apatite crystals were embedded in epoxy resin, the zircon and sphene grains in FEP-teflon. For apatite, zircon and sphene 1% nitric acid was used with 2.5–3 minute etching time (Burchart, 1972). In the case of zircon crystals the eutectic melt of NaOH–KOH–LiOH was used at a somewhat lower temperature ( $190^\circ\text{C}$ ) than suggested by the prescriptions of Zaun and Wagner (1985). Neutron irradiations were made at the nuclear reactor of the Austrian Universities at Vienna. The external detector method was used (Gleadow, 1981). The induced fission tracks in the mica detectors were etched by 40% HF for 40 min after irradiation. Spontaneous track counts were made in oil immersion under a Zeiss NU 2 microscope, with magnification of 1600 times. In the case of mica detectors dry optics of 800-time magnification was used.

The age was calculated on the basis of weighted average of the measured track density proportions, by the zeta-method (Hurford and Green, 1983) using zircon from the Fish Canyon Tuff and Tardree Rhyolite and apatite from Durango and the Fish Canyon Tuff. Reference ages of  $27.8 \pm 0.2$  Ma for the Fish Canyon Tuff,  $31.4 \pm 0.5$  Ma for the Durango apatite,  $16.2 \pm 0.6$  for the Buluk Member Tuff and  $58.7 \pm 1.1$  Ma for the Tardree Rhyolite have been adopted according to Hurford and Watkins (1978), Hurford and Green (1983), Hurford and Hammerschmidt (1985) and Green (1985). The errors were evaluated by classical procedures, i.e. by the double Poisson dispersion (Green, 1981).

## References

- Agnoli, F., Reisinger, J. and Mauritsch, H.J., 1989. Paläomagnetische Ergebnisse aus zwei Gosau-Vorkommen (Oberkreide). *Neues Jahrb. Geol. Paläontol. Monatsh.*, 1989: 265–281.
- Becker, L.P. and Schumacher, R., 1973. Metamorphose und Tektonik in dem Gebiet zwischen Stub- und Gleinalpe, Stmk. *Mitt. Geol. Ges. Wien*, 65(1972): 1–32.
- Blanckenburg, F. von, Villa, I.M., Baur, H., Morteani, G. and Steiger, R.H., 1989. Time calibration of a  $P$ – $T$  path from the western Tauern Window, eastern Alps: the problem of closure temperatures. *Contrib. Mineral. Petrol.*, 101: 1–11.
- Burchart, J., 1972. Fission track age determination of accessory apatite from the Tatra Mountains, Poland. *Earth Planet. Sci. Lett.*, 15: 418–422.
- Cassard, D., Feybesse, J.-L. and Lescuyer, J.-L., 1993. Variscan crustal thickening and late overstacking during the Namurian–Westphalian in the western Montagne Noire (France). *Tectonophysics*, 222: 33–53.
- Chauvet, A. and Dallmeyer, R.D., 1992.  $^{40}\text{Ar}/^{39}\text{Ar}$  mineral dates related to Devonian extension in the southwestern Scandinavian Caledonides. *Tectonophysics*, 210: 155–177.

- Choukroune, P., Gapais, D. and Merle, O., 1987. Shear criteria and structural symmetry. *J. Struct. Geol.*, 9: 525–530.
- Cliff, R.A., 1985. Isotopic dating in metamorphic belts. *J. Geol. Soc. London*, 142: 97–110.
- Clifton, H.E., 1969. Beach lamination: nature and origin. *Mar. Geol.*, 7: 553–559.
- Coney, P.J., 1980. Cordilleran metamorphic core complexes. *Mem. Geol. Soc. Am.*, 153: 7–35.
- Dallmeyer, R.D. and Gil-Ibarguchi, I., 1990. Age of amphibolitic metamorphism in the ophiolitic unit of the Morais allochthon (Portugal): implications for early Hercynian orogenesis in the Iberian Massif. *J. Geol. Soc. London*, 147: 873–978.
- Dallmeyer, R.D. and Keppie, J.D., 1987. Late Paleozoic tectono-thermal evolution of the southwestern Meguma Terrane, Nova Scotia. *Can. J. Earth Sci.*, 24: 1242–1245.
- Dallmeyer, R.D. and Takasu, A., 1992.  $^{40}\text{Ar}/^{39}\text{Ar}$  ages of detrital muscovite and whole rock slate/phyllite, Narragansett Basin, RI–MA, USA: implications for rejuvenation during very low-grade metamorphism. *Contrib. Mineral. Petrol.*, 110: 515–527.
- Dallmeyer, R.D., Neubauer, F., Handler, R., Müller, W., Fritz, H., Antonitsch, W. and Hermann, S., 1992.  $^{40}\text{Ar}/^{39}\text{Ar}$  and Rb/Sr mineral age controls for the pre-Alpine and Alpine tectonic evolution of the Austro-Alpine Nappe Complex, eastern Alps. *ALCAPA Field Guide, IGP/KFU Graz*, pp. 47–59.
- Dalrymple, G.P., 1981. Irradiation of samples for  $^{40}\text{Ar}/^{39}\text{Ar}$  dating using the Geological Survey TRIGA reactor. *U.S. Geol. Surv., Prof. Pap.*, 1176: 1–55.
- Dewey, J.F., 1988. Extensional collapse of orogens. *Tectonics*, 7: 1123–1139.
- Dewey, J.F., Helman, M.L., Turco, E., Hutton, D.H.W. and Knott, S.D., 1989. Kinematics of the western Mediterranean. *Geol. Soc. Spec. Publ.*, 45: 265–283.
- Ebner, F., 1986. Orbitoidensandsteine aus den Eckwirtschottern bei Oberdorf/Bärnbach. *Mitt. Naturwiss. Ver. Steiermark*, 116: 79–89.
- Echtler, H. and Malavieille, J., 1990. Extensional tectonics, basement uplift and Stephano–Permian collapse basin in a late Variscan metamorphic core complex (Montagne Noire, Southern Massif Central). *Tectonophysics*, 13: 17–50.
- England, Ph. and Molnar, P., 1990. Surface uplift, uplift of rocks, and exhumation of rocks. *Geology*, 18: 1173–1177.
- England, P.C. and Thompson, A.B., 1984. Pressure–temperature–time paths of regional metamorphism, Part I. Heat transfer during the evolution of regions of thickened continental crust. *J. Petrol.*, 25: 894–928.
- Etheridge, F.G. and Wescott, W.A., 1984. Tectonic setting, recognition and hydrocarbon potential of fan-delta deposits. In: E.H. Koster and R.J. Steel (Editors), *Sedimentology of Gravels and Conglomerates*. *Can. Soc. Pet. Geol. Mem.*, 10: 217–236.
- Frank, W., 1987. Evolution of the Austroalpine elements in the Cretaceous. In: H.W. Flügel and P. Faupl (Editors), *Geodynamics of the Eastern Alps*. Deuticke, Wien, pp. 379–406.
- Frank, W., Klein, P., Nowy, W. and Scharbert, S., 1976. Die Datierung geologischer Ereignisse im Altkristallin der Gleinalpe (Steiermark) mit der Rb/Sr-Methode. *Tschermaks Mineral. Petrogr. Mitt.*, 23: 191–203.
- Frank, W., Esterlus, M., Frey, I., Jung, G., Krohe, A. and Weber, J., 1983. Die Entwicklungsgeschichte von Stub- und Koralpe und die Beziehung zum Grazer Paläozoikum. *Berichte Hochschulschwerpunkt S15, Die früh-alpine Geschichte der Ostalpen*, 4: 263–293.
- Frank, W., Kralik, M., Scharbert, S. and Thöni, M., 1987. Geochronological Data from the Eastern Alps. In: H.W. Flügel and P. Faupl (Editors), *Geodynamics of the Eastern Alps*. Deuticke, Wien, pp. 272–279.
- Fritz, H., 1988. Kinematics and geochronology of Early Cretaceous thrusting in the northwestern Paleozoic of Graz (Eastern Alps). *Geodin. Acta*, 2: 53–62.
- Fritz, H., Neubauer, F. and Ratschbacher, L., 1990. Compression versus extension in the Paleozoic of Graz (Eastern Alps). *Zentralbl. Geol. Paläontol.*, 1990: 55–68.
- Froitzheim, N., 1992. Formation of recumbent folds during synorogenic crustal extension (Austroalpine nappes, Switzerland). *Geology*, 20: 923–926.
- Gleadow, A.J.W., 1981. Fission-track dating methods: what are the real alternatives? *Nucl. Tracks*, 5: 3–14.
- Gleadow, A.J.W. and Lovering, J.F., 1977. Geometry factor of external detectors in fission track dating. *Nucl. Track Detect.*, 1: 99–106.
- Gollner, H., Schirnik, D. and Tschelaut, W., 1987. The problem of the Southalpine clasts in the “Mittelsteirische Gosau”. In: H.W. Flügel and P. Faupl (Editors), *Geodynamics of the Eastern Alps*. Deuticke, Wien, pp. 156–163.
- Gräf, W., 1975. Ablagerungen der Gosau von Kainach. In: H.W. Flügel (Editor), *Die Geologie des Grazer Berglandes*. *Mitt. Abt. Geol. Paläontol. Bergbau Landesmus. Joanneum, Sonderh.*, 1: 83–102.
- Green, P.F., 1981. A new look at statistics in fission track dating. *Nucl. Tracks*, 5: 77–86.
- Green, P.F., 1985. A new look at statistics in fission track dating. *Nucl. Tracks*, 5: 77–86.
- Harland, W.B., Armstrong, R.L., Cox, A.V., Craig, L.E., Smith, A.G. and Smith, D.G., 1990. *A Geologic Time Scale 1989*. Cambridge University Press, Cambridge, 263 pp.
- Harrison, T.M., 1981. Diffusion of  $^{40}\text{Ar}$  in hornblende. *Contrib. Mineral. Petrol.*, 78: 324–331.
- Hasenhüttl, Chr. and Russegger, B., 1992. Niedriggradige Metamorphose im Paläozoikum von Graz. *Jahrb. Geol. Bundesanst.*, 135: 287–299.
- Holdaway, T.J.B., 1971. Stability of andalusite and the aluminum silicate phase diagram. *Am. J. Sci.*, 271: 97–131.
- Hsü, K.J., 1991. Exhumation of high-pressure metamorphic rocks. *Geology*, 19: 107–110.
- Hurford, A.J. and Green, P.F., 1983. The zeta age calibration of fission-track dating. *Chem. Geol. (Isot. Geosci. Sect.)*, 41: 285–317.
- Hurford, A.J. and Hammerschmidt, K., 1985.  $^{40}\text{Ar}/^{39}\text{Ar}$  and K–Ar dating of the Bishop and Fish Canyon Tuffs: cali-

- bration ages for fission track dating standards. *Chem. Geol. (Isot. Geosci. Sect.)*, 58: 23–32.
- Hurford, A.J. and Watkins, R.T., 1978. Fission track age of the tuffs of the Buluk Member, Bakate Formation, Northern Kenya: a suitable fission-track age standard. *Chem. Geol.*, 66: 209–216.
- Kollmann, H., 1965. Actaeonellen (Gastropoda) der ostalpinen Oberkreide. *Ann. Naturhist. Mus. Wien*, 71: 199–261.
- Krohe, A., 1987. Kinematics of Cretaceous nappe tectonics in the Austroalpine basement of the Koralpe region (eastern Austria). *Tectonophysics*, 136: 171–196.
- Kröll, A. and Heller, R., 1978. Die Tiefbohrung AFLING U 1 in der Kainacher Gosau. *Verh. Geol. Bundesanst.*, 1978: 23–34.
- Lal, D., Muralli, A.V., Rajan, R.S., Tammane, A.S., Lorin, J.C. and Pellas, P., 1968. Techniques for proper revelation and viewing of etch-tracks in meteoritic and terrestrial minerals. *Earth Planet. Sci. Lett.*, 5: 111–119.
- Le Pichon, X., Bergerat, F. and Roulet, M.J., 1988. Plate kinematics and tectonics leading to the Alpine belt formation. A new analysis. *Geol. Soc. Am. Spec. Pap.*, 218: 111–131.
- Lister, G.S. and Snoke, A.W., 1984. S–C mylonites. *J. Struct. Geol.*, 6: 617–638.
- Malavieille, J., 1993. Late orogenic extension in mountain belts: insights from the Basin and Range Province and the late Paleozoic Variscan belt. *Tectonics*, 12: 1115–1130.
- Miller, C., 1990. Petrology of the type locality eclogites from the Koralpe and Saualpe (Eastern Alps), Austria. *Schweiz. Mineral. Petrogr. Mitt.*, 70: 287–300.
- Mueller, W., Dallmeyer, R.D., Neubauer, F. and Thoeni, M., 1992. Chronology of Variscan metamorphic events and low grade Alpine overprint in the eastern Lower Austroalpine units: Rb/Sr and  $^{40}\text{Ar}/^{39}\text{Ar}$  age data (Wechsel and Raabalen unit, eastern Alps). *Terra Nova* 4, Abstr. Suppl., 2: 46.
- Nemec, W. and Steel, R.J., 1988. What is a fan delta and how do we recognize it? In: W. Nemeč and R.J. Steel (Editors), *Fan Deltas: Sedimentology and Tectonic Settings*. Blackie and Son, Glasgow, pp. 3–13.
- Neubauer, F., 1988. Bau und Entwicklungsgeschichte des Rennfeld-Mugel- und des Gleinalm-Kristallins (Ostalpen). *Abh. Geol. Bundesanst.*, 42: 1–137.
- Neubauer, F., Frisch, W. and Hansen, B.T., 1987. Time relations between Eoalpine metamorphism and thrusting: evidence from the Crystalline Basement of the Eastern Greywacke Zone. In: H.W. Flügel and P. Faupl (Editors), *Geodynamics of the Eastern Alps*. Deuticke, Wien, pp. 363–371.
- Neubauer, F., Müller, W., Peindl, P., Moyschewitz, G., Wallbrecher, E. and Thöni, M., 1992. Evolution of Lower Austroalpine units along the eastern margins of the Alps: a review. *ALCAPA Field Guide, IGP/KFU Graz*, pp. 97–114.
- Nievol, J., 1985. Die bruchhafte Tektonik entlang der Trofaiachlinie (Östliche Zentralalpen), Österreich. *Jahrb. Geol. Bundesanst.*, 127: 643–671.
- Pamouktchiev, A.I., 1970. Sur la presence de Maastrichtien près de Kainachbeckens (Autriche). *Ann. Univ. Sofia, Geol.*, 1/62(1967)/68: 47–52.
- Peindl, P., 1990. Variszische und alpidische Entwicklungsgeschichte des südöstlichen Raabalenkristallins (Steiermark). PhD thesis, Univ. of Graz, 252 pp.
- Petit, D., 1987. Criteria for the sense of movement on fault rock surfaces in brittle rocks. *J. Struct. Geol.*, 9: 597–608.
- Platt, J.P., 1986. Dynamics of orogenic wedges and the uplift of high-pressure metamorphic rocks. *Geol. Soc. Am. Bull.*, 97: 1037–1053.
- Platt, J.P., 1992. Exhumation of high-pressure rocks: a review of concepts and processes. *Terra Nova*, 5: 119–133.
- Radicati di Brozolo, F., Huneke, J.C., Papanastassiou, D.A. and Wasserburg, J., 1981.  $^{40}\text{Ar}/^{39}\text{Ar}$  and Rb–Sr age determinations on Quaternary volcanic rocks. *Earth Planet. Sci. Lett.*, 53: 233–244.
- Ratschbacher, L., 1986. Kinematics of Austro-Alpine cover nappes: changing translation path due to transpression. *Tectonophysics*, 125: 335–356.
- Ratschbacher, L. and Neubauer, F., 1989. West-directed decollement of Austro-Alpine cover nappes in the eastern Alps: geometrical and rheological considerations. *Geol. Soc. Spec. Publ.*, 45: 243–262.
- Ratschbacher, L., Frisch, W., Neubauer, F., Schmid, S.M. and Neugebauer, J., 1989. Extension in compressional orogenic belts: the eastern Alps. *Geology*, 17: 404–407.
- Ratschbacher, L., Wenk, H.-R. and Sintubin, M., 1991a. Calcite textures: examples from nappes with strain-path partitioning. *J. Struct. Geol.*, 13: 369–384.
- Ratschbacher, L., Frisch, W., Linzer, H.G. and Merle, O., 1991b. Lateral extrusion in the Eastern Alps, Part 2. Structural analysis. *Tectonics*, 10: 257–271.
- Reading, H.G., 1982. Sedimentary basins and global tectonics. *Proc. Geol. Assoc.*, 93: 321–350.
- Reading, H.G., 1986. *Sedimentary Environments and Facies*, 2nd ed. Blackwell, Oxford, 615 pp.
- Reindl, H., 1989. Das westliche Raabalenkristallin. PhD thesis, Univ. of Graz, 235 pp.
- Roddick, J.C., 1978. The application of isochron diagrams in  $^{40}\text{Ar}/^{39}\text{Ar}$  dating: a discussion. *Earth Planet. Sci. Lett.*, 41: 233–244.
- Roddick, J.C., Cliff, R.A. and Rex, D.C., 1980. The evolution of excess argon in Alpine biotites—a  $^{40}\text{Ar}/^{39}\text{Ar}$  analysis. *Earth Planet. Sci. Lett.*, 48: 185–208.
- Samson, S.D. and Alexander, E.C., Jr., 1987. Calibration of the interlaboratory  $^{40}\text{Ar}/^{39}\text{Ar}$  dating standard, Mmhb 1. *Chem. Geol. (Isot. Geosci. Sect.)*, 66: 27–34.
- Schirnik, D., 1994. Die Basiskonglomerate der Kainacher Gosau (Oberkreide), Ostalpen. PhD thesis, University of Graz, 198 pp.
- Seguret, M., Seranne, M. and Chauvet, A.B.M., 1989. Collapse basin: a new type of extensional sedimentary basin from the Devonian of Norway. *Geology*, 17: 127–130.

- Simpson, C. and Schmid, S.M., 1983. An evaluation of criteria to deduce the sense of movement in sheared rocks. *Geol. Soc. Am. Bull.*, 94: 1281–1288.
- Steiger, R.H. and Jäger, E., 1977. Subcommittee on geochronology convention on the use of decay constants in geo- and cosmochronology. *Earth Planet. Sci. Lett.*, 36: 359–362.
- Teichmüller, M., 1980. Inkohlungsgrad-Bestimmung an Kohlen- und Mergelsteinproben aus der Kainacher Gosau (Obersanton–Untercampan) des Grazer Berglandes. *Berichte Hochschulschwerpunkt S15, Die frühalpiner Geschichte der Ostalpen*, 2: 102–104.
- Thöni, M. and Jagoutz, E., 1992. Some new aspects of dating eclogites in orogenic belts: Sm–Nd, Rb–Sr, and Pb–Pb isotopic results from the Austroalpine Saualpe and Koralpe type-locality (Carinthia/Styria, southeastern Austria). *Geochim. Cosmochim. Acta*, 56: 347–368.
- Tollmann, A., 1987. The Alpidic Evolution of the Eastern Alps. In: H.W. Flügel and P. Faupl (Editors), *Geodynamics of the Eastern Alps*. Deuticke, Wien, pp. 361–378.
- Tullis, J. and Yund, R.A., 1985. Dynamic recrystallization of feldspar: a mechanism for ductile shear zone formation. *Geology*, 13: 238–241.
- Van Hinte, J.E., 1965. Remarks on the Kainach Gosau (Styria, Austria). *K. Ned. Akad. Wet. Proc., Ser. B.*, 68: 72–92.
- Wagreich, M., 1991. Subsidenzanalyse an kalkalpinen Oberkreideseerien der Gosau-Gruppe (Österreich). *Zentralbl. Geol. Paläontol. Teil I*, 1990/II: 1645–1657.
- Wagreich, M., 1995. Subduction tectonic erosion and Late Cretaceous subsidence along the northern Austroalpine margin (Eastern Alps, Austria). In: F. Neubauer, F. Ebner and E. Wallbrecher (Editors), *Tectonics of the Alpine–Carpathian–Pannonian Region*. *Tectonophysics*, 242: 63–78.
- Wescott, W.A. and Etheridge, D.K., 1980. Fan delta sedimentology and tectonic settings—Yallahs fan delta, southeast Jamaica. *Am. Assoc. Pet. Geol. Bull.*, 64: 374–399.
- York, D., 1969. Least squares fitting of a straight line with correlated errors. *Earth Planet. Sci. Lett.*, 5: 320–324.
- Zaun, P.E. and Wagner, G.A., 1985. Fission-track stability in zircon under geological conditions. *Nucl. Tracks*, 10: 303–307.